Mesoscale molecular network formation in amorphous organic materials

Brett M. Savoie[a,1], Kevin L. Kohlstedt[a], Nicholas E. Jackson[a], Lin X. Chen[a,b], Monica Olvera de la Cruz[a], George C. Schatz[a], Tobin J. Marks[a,1], and Mark A. Ratner[a,1]

[a]Department of Chemistry, Northwestern University, Evanston, IL 60208; and [b]Chemical Sciences and Engineering Division, Argonne National Laboratory, Lemont, IL, 60439

Contributed by Tobin J. Marks, June 2, 2014 (sent for review April 9, 2014; reviewed by Roald Hoffmann, Michael Brenner, and James Durrant)

High-performance solution-processed organic semiconductors maintain macroscopic functionality even in the presence of microscopic disorder. Here we show that the functional robustness of certain organic materials arises from the ability of molecules to create connected mesoscopic electrical networks, even in the absence of periodic order. The hierarchical network structures of two families of important organic photovoltaic acceptors, functionalized fullerenes and perylene diimides, are analyzed using a newly developed graph methodology. The results establish a connection between network robustness and molecular topology, and also demonstrate that solubilizing moieties play a large role in disrupting the molecular networks responsible for charge transport. A clear link is established between the success of mono and bis functionalized fullerene acceptors in organic photovoltaics and their ability to construct mesoscopically connected electrical networks over length scales of 10 nm.

soft materials | disordered properties | charge generation

The discovery that organic semiconductors can complement, or even replace, more expensive/less processable inorganic semiconductors in many applications has spurred intense research for several decades (1). This led to the realization of devices where organics act as one, or all, of the components in transistor, battery, light-emitting diode, photovoltaic, and artificial photosynthetic technologies (2). All of these applications rely on the efficient mesoscopic (10–1,000 nm length scale) transport of charge or energy through space, whereas the fundamental design unit for these systems is the single molecule (~1 nm length scale). The successful function of these devices thus lies in the ability to bridge these length scales through the construction of efficient electrical molecular networks in the condensed phase. In this context, the challenge for materials scientists is to develop molecular descriptors that are predictive for macroscopic observables, such as charge mobility (3), exciton diffusion (4), or charge generation (5).

To close this understanding gap, it will be necessary to develop methodologies that go beyond the traditional formulation of quantum chemistry, which begins with accurate single-molecule properties and extrapolates outward, to frameworks that establish the hierarchical importance of the many possible intermolecular interactions in structurally disordered materials (6–9). In this work, we show how network theory can be combined with quantum chemistry to describe the mesoscopic percolative behavior of technologically relevant organic electron acceptors. The network framework enables the connectivity of the quantum transport states in these materials to be described on the 10–1,000 nm length scale as a function of molecular identity and structural disorder. By evaluating how the transport networks transform with structural disorder and molecular identity, we elucidate the connection between network robustness and molecular topology.

Nature offers a template for how relatively small molecular units can be combined to transport charge and energy rapidly over large distances. For instance, the biochemical machinery of both photosynthesis (10) and cellular respiration (11) depends on the intricate distribution and alignment of chromophores and redox centers throughout many proteins and membranes. This cellular machinery, which sustains most life on Earth, highlights the central importance of molecular alignment in both energy and space to facilitate energy and charge transport within networks of molecules. In both natural examples, however, the orientations of the molecules comprising the transport network are precisely controlled by protein scaffolding, but in synthetic materials such a level of control is currently unattainable. This represents a challenge for the rational design of materials for energy and charge transport, because orientational disorder must be considered, and the crystal structure, even when obtainable, may have little bearing on the microstructure of the actual film (12–14). This challenge is further accentuated for solution-processable materials, where film disorder is widely recognized as intrinsic to the deposition technique (6, 15). Moreover, the chemical moieties responsible for solubilizing organic semiconductors, such as linear and branched alkyl substituents, do not contribute to the quantum states responsible for optoelectronic functionality (species such as in Fig. 1), but act instead as insulators in a semiconducting film. As we show below, these moieties play a larger role than even structural disorder in ultimately disrupting the mesoscopic electrical networks responsible for charge transport.

Elementary Network Analysis

Concepts from graph theory have been used to analyze problems as seemingly disparate as tracing genetic inheritance (16), evaluating the Internet's robustness to power outages (17), and

Significance

Rapid and robust charge transport in soft matter semiconductors enables technologies such as photovoltaics, transistors, and light-emitting diodes. However, even at a conceptual level it remains unresolved what transport limitations are engendered by the structural disorder typical of soft materials. A graph methodology has been developed to quantify the mesoscopic electrical connectivity of clusters of molecules and its susceptibility to structural disorder. It is observed that some materials exhibit the capacity to regularly form conductive networks that percolate the material volume, even in the absence of periodic order. Moreover, the network properties of electrically percolating materials are qualitatively distinguished from nonpercolating materials, although both are comprised of ostensibly similar molecular units in terms of chemical structure, energy levels, and dimensionality.

Author contributions: B.M.S., L.X.C., M.O.d.l.C., G.C.S., T.J.M., and M.A.R. designed research; B.M.S., K.L.K., and N.E.J. performed research; B.M.S. analyzed data; and B.M.S. wrote the paper.

Reviewers: R.H., Cornell University; M.B., Harvard University; and J.D., Imperial College.

The authors declare no conflict of interest.

[1]To whom correspondence may be addressed. Email: brettsavoie@u.northwestern.edu, t-marks@northwestern.edu, or ratner@northwestern.edu.

This article contains supporting information online at www.pnas.org/lookup/suppl/doi:10.1073/pnas.1409514111/-/DCSupplemental.

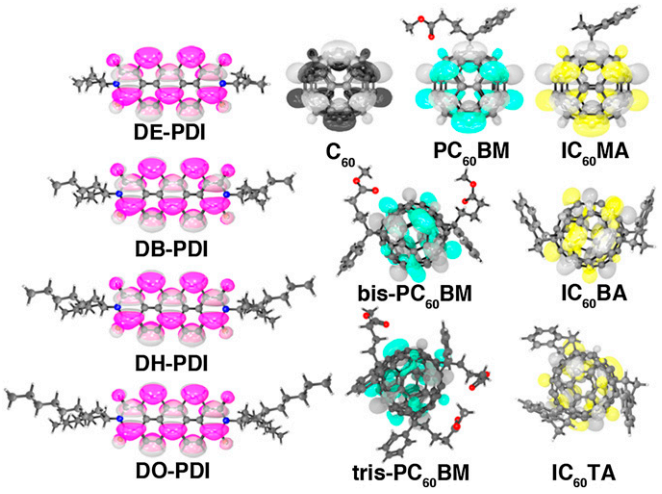

Fig. 1. The molecular structure and LUMOs of several organic electron acceptors used in organic photovoltaic cells. With the exception of C_{60}, all of the acceptors have saturated hydrocarbon solution-processing substituents that contribute little to the LUMO that mediates charge transport. Moreover, the LUMO topology is essentially identical to that of the unfunctionalized parent molecule: All fullerene derivatives have spherical LUMOs, and all PDI derivatives have planar LUMOs.

characterizing the electronic structure of molecules (18). A graph, **G**, is a general object easily visualized as in Fig. 2*A*. This intuitive object is formally defined by lists of vertices (**V**) and edges (**E**); together **V** and **E** contain all of the pairwise relationships that define **G**. In graph theory, the concept of an edge is generalized to be compatible with any dimension of comparison. For example, if the vertices represent atoms, then the edges could represent bonds, nearest neighbors, or like elements, depending on the problem of interest (19, 20). All vertex and edge relationships are succinctly contained within the weighted adjacency matrix, **A**, for the graph (Fig. 2*A*), where **A** is expressed in the basis of vertices, and the elements A_{ij} express the magnitude of each edge in the graph. Depending on the property that the edges represent, A_{ij} might take binary, integer, or continuous values.

The hierarchical importance of interactions between vertices can be assessed through simple operations on the adjacency matrix of the graph (Fig. 2*A*). In this study we define a simple networking algorithm, N(**X;R**), that returns the subnetworks within the matrix **X** that satisfy the list of connectivity conditions, **R**. Formally, N is a crawling algorithm that partitions the vertices of the graph into subgroups (networks) based upon the connectivity conditions (*SI Appendix, Methods*). The operation of N on **X** produces a variable number of subnetworks, depending on the permissiveness of the criteria within **R**.

As an example, Fig. 2*A* shows an application of the networking algorithm using the minimal criteria that an edge (of any magnitude) exists between two vertices. This returns two subnetworks, revealing that the set {a-j} is comprised of two unconnected systems. Additional information can be extracted by noting that the graph includes edges with capacities between 0 and 3. The result of applying the networking algorithm for varying thresholds on the edge capacity results in varying numbers of subnetworks. As the connectivity threshold is increased from $A_{ij} > 0$ to $A_{ij} > 2$, the networks fragment due to the smaller number of connections in the set, and a smaller number of independent pathways connect the vertices of each network.

The networks in Fig. 2 have intentionally been drawn in a nonintuitive spatial distribution to reflect the similarly counterintuitive relationship between spatial proximity and electrical connectivity in many real systems (21). A major finding of the present study is that ostensibly proximate quantum states can be electrically inaccessible in the amorphous phase, depending upon the topology, state degeneracy, and degree of functionalization of the molecular repeat unit.

Molecular Networks

Graphical approaches in chemistry have a rich history for describing the electronic structure of molecules beginning with Kekule (22), and continued by Pauling (23), Clar (24), Heilbronner (25), and many others (26, 27). Burdett and Lee first showed that graphical operations on tight-binding Hamiltonians could be used to understand the density of states of solids and clusters (28). We now show that by a simple, powerful extension, graph approaches can be used to describe mesoscopic relationships among interacting molecules.

In the weak coupling regime, charge transfer between molecules is mediated by the energy difference and electronic coupling of molecular orbitals (MOs; Fig. 1; ref. 29). The network

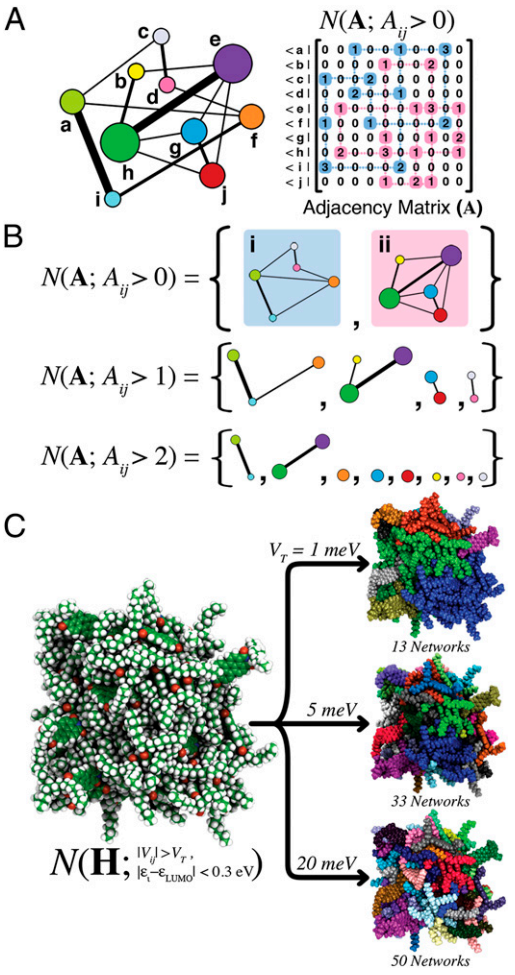

Fig. 2. (*A, Left*) Generalized graph of vertices (a–h) and edges (lines). The edge thickness corresponds to the strength of the connection between vertices, and vertex radii are scaled according to the number of finite capacity edges per vertex. (*A, Right*) Pedagogic representation of the network analysis algorithm N acting on the adjacency matrix **A** for the graph on the *Left*. (*B*) Returned networks for finite capacity ($A_{ij} > 0$), edge capacity greater than 1 ($A_{ij} > 1$), and edge capacity greater than 2 ($A_{ij} > 2$). (*C, Left*) Snapshot of 64 DO-PDI molecules from a MD trajectory. Network analysis is performed using states within 0.3 eV of the DO-PDI LUMO, and a variable electronic coupling threshold, V_T. (*C, Right*) Returned networks for a range of thresholds: V_T values of 1, 5, and 20 meV. In each case, distinct electrical networks are given a unique color, and the total number of networks is specified beneath each cluster.

analysis developed above for the generic graph in Fig. 2 can be extended to arrays of molecules by realizing that, when expressed in the MO basis, the electronic tight-binding Hamiltonian, **H**, carries the same structure as the adjacency matrix,

$$\mathbf{H} = \sum_i \varepsilon_i |\phi_i\rangle\langle\phi_i| + \sum_{i,j} V_{ij} |\phi_i\rangle\langle\phi_j|. \quad [1]$$

Here ϕ_is are the molecular orbitals, indices i and j run over all molecular orbitals on all molecules in the system, ε_i is the energy of ϕ_i, and V_{ij} is the electronic coupling between orbitals ϕ_i and ϕ_j. In the MO basis, the magnitude of the off-diagonal elements of **H** reflects the degree of mixing between molecular orbitals on different molecules in the mesoscopic system. Because all that is required to apply the network analysis is a unitary basis set transformation from the system eigenbasis to a localized molecular basis (of which the MO basis is the simplest), the model chemistry represented by **H** can be chosen to suit the application.

Expressed in the MO basis, **H** contains the MO energy differences and couplings necessary to enumerate the possible pathways for charge transfer. Network analysis of the form $N(\mathbf{H};\mathbf{R})$ can thus be generalized to evaluate the hierarchical electrical connectivity of arbitrary arrays of molecules. To identify the networks capable of transporting charge, we use simple conditions for **R** based on the energy differences and couplings between MOs. All of the materials studied in this work are used as electron acceptors, so only MOs within 0.3 eV of the vacuum lowest unoccupied molecular orbital (LUMO) level of each molecule are included in each network ($|\varepsilon_i - \varepsilon_{LUMO}| < 0.3$ eV). The connectivity between MOs is then determined by a variable threshold, V_T, for the electronic coupling, and MOs are considered connected when the condition $|H_{ij}| > V_T$ is satisfied.

Fig. 2*C* shows an example of molecular network analysis on a cluster of 64 *N,N′*-Bis(1-octylnonyl)perylene-3,4,9,10-tetracarboxylic diimide (DO-PDI) molecules (see Fig. 3*C* for all molecular structures, and the *SI Appendix* for formal names). It is immediately apparent that the networking algorithm reveals the hierarchical connectivity of molecules within the cluster in an intuitive fashion. Using the very weak threshold V_T = 1 meV, several independent networks already exist within the cluster. Stronger molecular connections are returned by increasing the V_T, from 1 to 5 and 20 meV, respectively, from which it can be observed that network fragmentation occurs [maximum fragmentation occurs, in this case, when $N(\mathbf{H};\mathbf{R})$ = number of molecules]. As shown below, the dependence of network fragmentation on the coupling threshold can be used to evaluate the relative robustness to disorder of electron motion within the cluster and the probability that a percolation path for charge transport spans the cluster volume.

We now present the results of the network analysis for two families of important organic electron acceptors: substituted perylene diimides (PDI) and C_{60} fullerenes. Fullerene derivatives are preeminent acceptors in virtually all high-performance organic photovoltaic (OPV) cells (30). Monofunctionalized fullerenes such as $PC_{60}BM$ (Fig. 1) are high-mobility *n*-type semiconductors, despite forming disordered glassy films (12), and bis and tris-functionalized fullerenes attract interest due to their lower electron affinities and potential to sustain higher device open-circuit voltages in solar cells (31, 32). PDI derivatives have been studied as promising replacements for fullerenes in OPVs (33), as they are inexpensive, robust, and possess highly

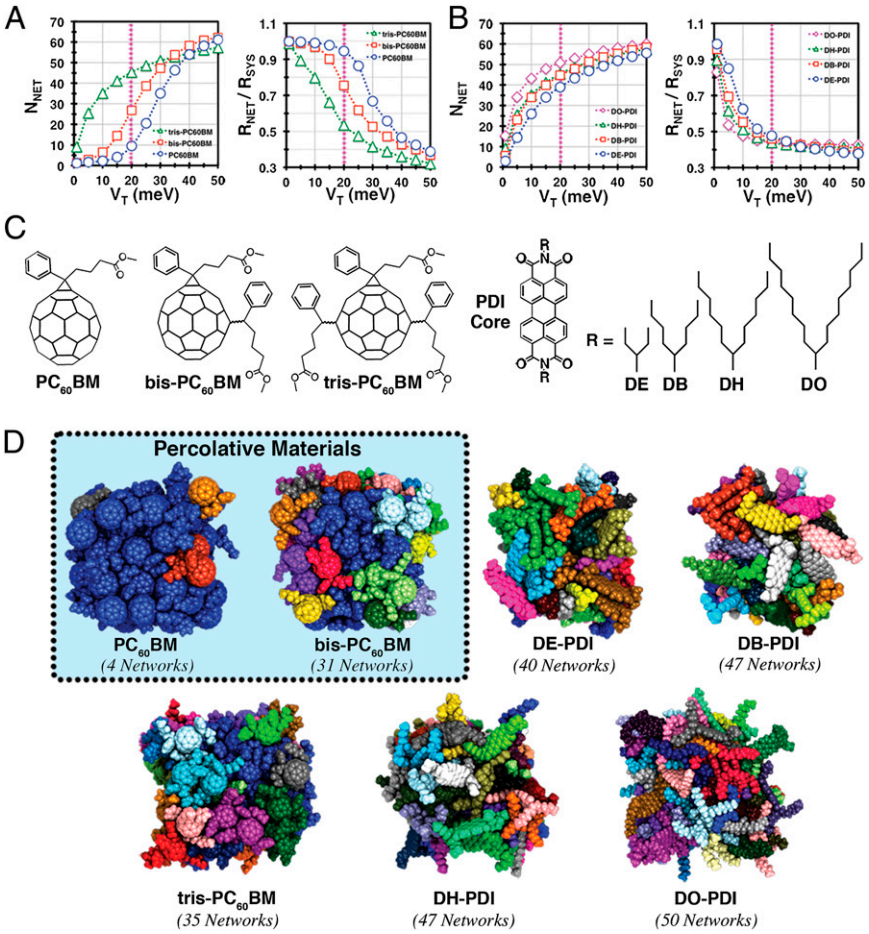

Fig. 3. (*A, Left*) Number of networks, N_{NET} in $PC_{60}BM$-based systems as a function of electronic coupling threshold. (*A, Right*) Ratio of the radius of gyration of the largest network to the total system radius of gyration, as a function of the electronic coupling threshold. (*B, Left*) Number of networks, N_{NET}, in PDI derivatives as a function of electronic coupling threshold V_T. (*B, Right*) Ratio of the radius of gyration of the largest network to the total system radius of gyration, as a function of V_T. (*C*) Molecular structures of the substituted fullerenes and PDIs. Many regioisomers are possible for bis and tris-PCBM; see *SI Appendix* for a full discussion. (*D*) Subnetworks for a sample snapshot of each system, with a coupling threshold, V_T, of 20 meV. In each case, distinct electrical networks are given a unique color, and the total number of networks is specified beneath each cluster. The pink lines in *A* and *B* denote the threshold value visualized in *D*. $PC_{60}BM$ and bis-$PC_{60}BM$ materials are highlighted as the only materials whose largest electronic network percolates the cluster volume at the 20-meV threshold.

tunable solubility and orbital energetics (34). In both families of materials, the attachment of side chains renders the materials soluble in common organic solvents (requisite for solution phase film growth), and in the resulting films, the side chains contribute negligibly to the orbitals mediating charge transfer (Fig. 1).

The network methodology developed in the previous section was used to interrogate the mesoscale electrical connectivity of PDI derivatives with varying length side chains, from dioctyl (DO-PDI) to dihexyl (DH-PDI), dibutyl (DB-PDI), and diethyl (DE-PDI), as well as C_{60} derivatives, $PC_{60}BM$, bis-$PC_{60}BM$, and tris-$PC_{60}BM$, that differ by the number of attached side chains (Fig. 3*C*). For each of the seven materials, a 64-molecule cluster was simulated using classical molecular dynamics (MD) in an isobaric–isothermal ensemble. The central role of surface effects in both OPVs and organic transistors makes it necessary to simulate finite clusters rather than bulk periodic materials (1, 7). The network analysis for each material was then performed on 50 snapshots collected from five independent MD trajectories (the size dependence, role of surface molecules, convergence behaviors are discussed in the *SI Appendix*). These simulations were used to assess each material's capacity to form mesoscale networks in disordered environments. (See *SI Appendix, Methods* for additional details.)

Network analysis for each material within the $PC_{60}BM$ family was performed over a V_T ranging from 1 to 50 meV. The magnitude of the coupling element between MOs, V_{ij}, determines the upper limit for the rate of charge transfer between molecules [$\tau^{-1} \sim 2\pi\ \hbar^{-1}\ V_{ij}^2$, taking the density of states factor to be one state per electron volt (eV)], which can be used to estimate the timescale for charge movement through a given network. For example, a coupling of 1 meV corresponds to a transfer time between molecules of ∼0.7 ns, and a coupling of 20 meV decreases the transfer time to ∼1.5 ps, making the process potentially competitive with nuclear reorganization. For an organic solar cell, the injected charge must traverse several nanometers within a few picoseconds to avoid geminate recombination (35). Thus, percolating networks with thresholds >1 meV, (and probably even >20 meV) are necessary to guarantee this possibility. Electronic couplings less than this, even neglecting other considerations, are simply not strong enough to facilitate the transfer. Fig. 3*A* shows the number of independent (unconnected) networks as a function of V_T for the C_{60} derivatives. In this analysis, fewer networks implies greater electrical connectivity throughout the cluster, and therefore favorable mesoscale charge transport. There is also a conceptual connection between network fragmentation behaviors and Klein and Randić's idea of graphical resistance (36). Across the fullerene series, increasing functionalization unambiguously leads to greater network fragmentation. In the case of the highly substituted tris-$PC_{60}BM$ material, fragmentation even occurs at the smallest investigated values of V_T (for V_T = 1 meV, ∼3 networks exist on average).

To establish the degree to which fragmentation correlates with an actual spatial contraction of the transport network, we evaluated the radius of gyration, R_{NET}, of the largest network in each system

$$R_{NET}^2 = \frac{1}{N}\sum_{i}^{N} |r_i - \langle r_{NET}\rangle|^2, \qquad [2]$$

where the index i runs over all N atoms in the largest network, r_i is the position of atom i, and r_{NET} is the network centroid. Similarly, the radius of gyration of the total system, R_{SYS}, was calculated according to Eq. **2** while allowing the summation to run over all atoms in the cluster. The ratio R_{NET}/R_{SYS}, hereafter referred to as the percolation ratio, provides a metric for the degree to which the largest network percolates the cluster.

Fig. 3*A* shows the percolation ratio as a function of V_T for the present C_{60} derivatives. The network characteristics of the tris-$PC_{60}BM$ material are again qualitatively distinguished from the mono and bis materials by a precipitous decline in percolation behavior above the 1-meV threshold. The failure to produce percolating networks at even small couplings suggests that coherent electron transport between tris-$PC_{60}BM$ molecules is strongly suppressed in this material, and that electron transfer is limited to thermally activated nuclear rearrangement. This qualitative distinction between $PC_{60}BM$ and bis-$PC_{60}BM$ relative to tris-$PC_{60}BM$ is surprising in light of the incremental nature of the substitution: the tris-material, although energetically semiconducting with a band gap similar to the other materials, behaves mesoscopically as an insulator due to poor intermolecular coupling and high energetic dispersion. This is also born out experimentally by the exceptionally poor electron mobility reported for tris-$PC_{60}BM$ ($\sim 4 \times 10^{-9}$ $cm^2\ V^{-1}\ s^{-1}$) relative to $PC_{60}BM$ ($\sim 1 \times 10^{-3}$ $cm^2\ V^{-1}\ s^{-1}$) and bis-$PC_{60}BM$ ($\sim 1 \times 10^{-4}$ $cm^2\ V^{-1}\ s^{-1}$), assayed by space-charge limited current measurements (37). Our simulations can also be compared with the corresponding organic solar cells, whose filamentous acceptor domains have dimensions comparable to our simulated clusters (30). OPV devices using the tris-$PC_{60}BM$ acceptor show consistently poor photocurrent production in all known device configurations (37, 38), suggesting that tris-$PC_{60}BM$ fails to facilitate the electron–hole separation necessary for photocurrent production; whereas, efficient devices using both mono and bis-$PC_{60}BM$ acceptors have long been known (31).

The same network analyses that were performed on the C_{60} derivatives were next performed on the family of PDI acceptors (Fig. 3*B*). Qualitatively, the network structure of the PDI materials shares similar nonpercolative features with the tris-$PC_{60}BM$ networks. Even at the permissive 1-meV coupling threshold, the derivatives with the longest side chains, DO-PDI and DH-PDI, are comprised of many networks, and none of the materials efficiently percolate the cluster volume for $V_T > 1$ meV.

The topology of each class of molecules is also reflected in the shape of the networks that each molecule forms. This is rigorously quantified by calculating the orientational correlation factors between the molecules in each network (*SI Appendix*, Figs. S4 and S5), but even visual inspection of Fig. 3*D* shows that the planar and spherical topologies of PDI and C_{60} are inherited in the network topologies as stacks and globules, respectively. The orientational correlation data also demonstrate that electrical connections between PDI derivatives are limited solely to stacked orientations, in agreement with the columnar structures and strong mobility anisotropy experimentally associated with this class of materials (39, 40). As we show below, however, the restricted orientational space for establishing connections between PDIs leads to an unexpected fragilizing effect on the mesoscopic electrical networks.

Network Robustness

Comparing the stacked PDI networks with the globular networks formed by the C_{60} derivatives, we speculate that the dimensionality of the networks influences their fragility with respect to structural disorder. As elaborated below, fragility can be quantified by two complementary measures: (*i*) the average number of connections per molecule in each material (network fragility) and (*ii*) the spatial contraction of the largest network with respect to fragmentation (percolation fragility).

Fig. 4*A* shows the average number of connections per molecule, N_C, across each series of materials. These numbers should be interpreted while keeping in mind that a continuous unfragmented network can only be formed if the average molecule has ∼2 connected neighbors (see *SI Appendix* for more detail). Minimally connected systems ($N_C \sim 2$) are "fragile," however, because they cannot tolerate any pairwise disruptions without network fragmentation. Networks comprised of multiply connected molecules ($N_C > 2$), possess built-in redundancies for charge transport, and can tolerate pairwise disruptions without fragmentation. This is confirmed by observing that the coupling threshold at which the N_C of each material falls below ∼2 corresponds to the onset of network fragmentation in Fig. 3 *A* and *B*.

It is also evident that within each family and across all values of V_T, increasing functionalization is accompanied by fewer connections per molecule and increasing fragmentation susceptibility. From this dataset we can also infer that even when the PDI derivatives efficiently form stacks, the networks remain fragile. The geometric constraints of stacking essentially limit their coupling to two neighbors, with the result that none of the N_C values for PDI derivatives rise much above ~2 for any appreciable value of the coupling threshold. This also correlates with the counterintuitive result that the best fullerene replacements in organic solar cells have been PDI units designed to disrupt stacking via covalent dimerization (41–43). In addition to promoting miscibility with the donor, these nonplanar structures likely emulate the superior percolative properties of spherical fullerenes.

The ability of a material to sustain network fragmentation while maintaining percolation can be quantified by the magnitude of $\frac{dR_{NET}}{dN_{NET}}$ (Fig. 4*B*), representing the rate of largest network spatial contraction versus fragmentation (percolation fragility). For example, it is unnecessary for the fragmentation transitions shown in Fig. 3 *A* and *B* to also correspond to percolation transitions, because the latter are defined only by the spatial extent of the largest networks. We expect that some materials may accommodate fragmentation while retaining transport capability (6), with the most favorable scenario being that fragmentation occurs while leaving a large percolating network intact (7). Investigating the hypothesis that percolation fragility has a topological contribution from the molecular units, we compare the percolation behavior of the C_{60} and PDI derivatives in Fig. 4*B*, and observe a clear difference in how the largest networks of each family respond to fragmentation. The slower decline in the percolation ratio of the C_{60} derivatives with fragmentation suggests that the largest networks in these clusters contract more slowly than those of the PDI derivatives. This feature is also preserved within each family, despite the varying degree of functionalization, which clearly demonstrates the topological contribution to percolation fragility.

Furthermore, the percolation fragility quantified in Fig. 4*B* also suggests that molecular topology impacts the distribution of weak/broken connections throughout the percolating network. Fragile percolating networks appear to accumulate weak connections at core and branch vertices (e.g., in stacked PDI networks, with only ~2 connections per molecule, every molecule serves as a branch point); whereas, robust percolating networks distribute weak connections to the periphery or in local aggregates that prevent total collapse (e.g., in Fig. 3*D*, both the $PC_{60}BM$ and bis-$PC_{60}BM$ materials fragment first along the surface while retaining central percolating networks; see *SI Appendix* for further discussion). These results plausibly suggest that materials can be designed with specific percolation properties for applications such as OPV cells and organic field-effect transistors, where performance depends on achieving electrical percolation in minimally processed, usually highly disordered, films (7, 39).

In principle, the susceptibility of electrical percolation to structural disorder is inherent in device work as the performance variance across devices, and the sensitivity of performance to processing. Neglecting other considerations, materials that form fragile networks should generally be more demanding to work with, exhibit lower performance stability, and systematically show greater performance variance across devices. Robustness considerations are thus of tremendous importance for practical device work, although little discussed, and almost never considered during the design process. To our knowledge, the graph methodology developed here is the first means of quantifying this property for soft semiconductors.

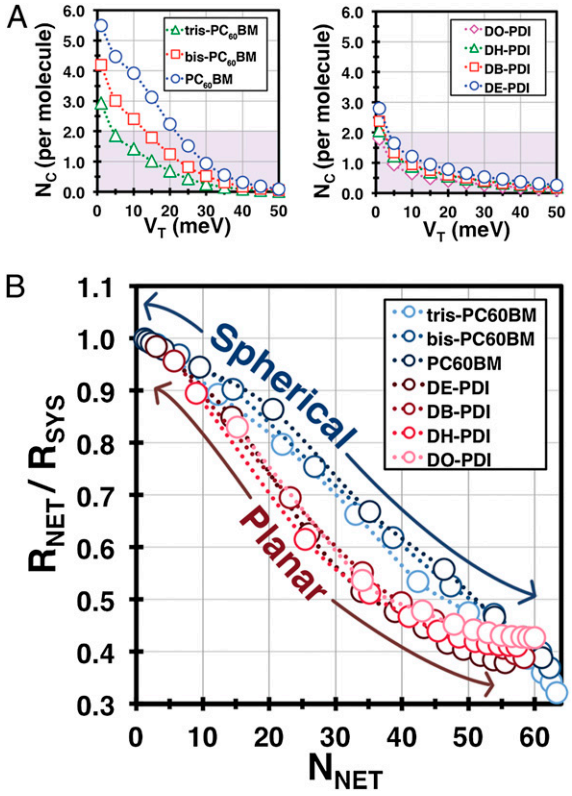

Fig. 4. (*A, Left*) Average number of connections per molecule, N_C, in C_{60} derivatives as a function of the electronic coupling threshold (V_T). (*Right*) N_C as a function of coupling threshold for the PDI derivatives. Shaded areas indicate nonpercolative conditions. (*B*) Number of networks (N_{NET}) versus the percolation ratio (R_{NET}/R_{SYS}) compared across all materials. Lines added as a guide to the eye, "spherical" refers to the C_{60} derivatives (in blue) and "planar" to the PDI derivatives (in red).

Connections Between Molecular Networks, Percolation Theory, and Charge Transport

The graph methodology developed here can be considered to a unification of traditional percolation models with the quantum details of molecular semiconductors. As applied to bicontinuous bulk heterojunctions, percolation models typically assume that the nuclear coordinates are congruent with the electronic coordinates and that transport within each phase can be modeled as an effective medium (44–46). Both assumptions have proven successful in different contexts, but are invalid for solution-processed semiconductors where charge transport bears both orientational anisotropy and spatial inhomogeneity, and the charge carrier wave functions are highly localized on conjugated moieties. By working within a basis of transport states, this approach remedies both shortcomings and maps the powerful machinery of percolation theory onto the molecular details of electronic structure.

We have highlighted here that graph analysis provides complementary information to traditional charge-transport simulations (47, 48), including the spatial distribution of transport bottlenecks, directionality of transport networks, percolation behaviors, and the vulnerability of percolation to structural disorder. The natural next step will be to use the network information to generate more accurate charge transport models. The clearest connection between the networks and transport lies in understanding $N(\mathbf{H};\mathbf{R})$ to represent the subspace of efficient pathways for charge transport, whose traversal timescale is determined by the couplings and the energy differences defined in $\mathbf{R}$. For hopping transport, the dynamical nature of the networks is germane because the timescale of transfer is slow relative to the nuclear motion. For coherent transport, the snapshot network structure supplies information about the transport pathways that are instantaneously available. In each case, network percolation is a necessary (although not sufficient) criteria for efficient transport that can be screened for during design. Moreover, the spatial connectivity information supplied by the

network structure is usually a fitted parameter in traditional variable range and Gaussian disorder models, which limits these to a posteriori use. Significant work by Baumeir et al. has also shown that network structures can be used to produce accurate first principles models of transport that are scalable to macroscopic applications (49).

Conclusions

Sustainable progress in organic semiconductor design ultimately requires a quantitative predictive understanding of the way materials transport properties respond to structural disorder. This is especially true of solution-processed materials and for applications such as solar cells and transistors where performance has proven remarkably sensitive to mesoscopic morphological features. However, inexpensive processing and structural disorder need not be incompatible with robust performance; as this work demonstrates, it is possible for some molecules to form mesoscopically connected networks even in the absence of periodic order. This represents a materials design paradigm focused on stochastic robustness and electrical network assembly that complements traditional process-engineering and crystal-packing studies.

For mesoscopic phenomena, such as charge generation and transport, where functionality arises from charge moving in space, understanding the spatial connectivity of molecular states is critical for evaluating functionality. The molecular network serves as an intuitive, uniquely defined object that expresses all accessibility relationships among molecules in the condensed phase, thus conveying physical content that includes, but goes beyond, density of states and bandwidth analyses, with obvious applications for models of charge and energy transport. Work is currently underway investigating the capacity of network analysis for materials screening and extending the approach to polymeric and binary materials.

ACKNOWLEDGMENTS. This work was supported as part of the Argonne-Northwestern Solar Energy Research Center, an Energy Frontier Research Center funded by the US Department of Energy, Office of Science, Office of Basic Energy Sciences, under Award DE-SC0001059. K.L.K. and M.O.d.l.C. thank the Air Force Office of Scientific Research Multidisciplinary University Research Initiative Grant FA9550-11-1-0275 for their support. N.E.J. thanks the National Science Foundation (NSF) for the award of a graduate research fellowship (NSF DGE-0824162). M.A.R. acknowledges the Israel-US Binational Science Foundation Grant 2011509 for its support. B.M.S. thanks the Northwestern Materials Research Science and Engineering Center (NSF DMR-1121262) for a graduate research fellowship.

1. Marks TJ (2010) Materials for organic and hybrid inorganic/organic electronics. *MRS Bull* 35(12):1018–1027.
2. Forrest SR (2004) The path to ubiquitous and low-cost organic electronic appliances on plastic. *Nature* 428(6986):911–918.
3. Saeki A, Koizumi Y, Aida T, Seki S (2012) Comprehensive approach to intrinsic charge carrier mobility in conjugated organic molecules, macromolecules, and supramolecular architectures. *Acc Chem Res* 45(8):1193–1202.
4. Scholes GD, Rumbles G (2006) Excitons in nanoscale systems. *Nat Mater* 5(9):683–696.
5. Bakulin AA, et al. (2012) The role of driving energy and delocalized states for charge separation in organic semiconductors. *Science* 335(6074):1340–1344.
6. Noriega R, et al. (2013) A general relationship between disorder, aggregation and charge transport in conjugated polymers. *Nat Mater* 12(11):1038–1044.
7. Bartelt J, et al. (2013) The importance of fullerene percolation in the mixed regions of polymer–fullerene bulk heterojunction solar cells. *Adv Energy Mater* 3:364–374.
8. Laughlin RB, Pines D, Schmalian J, Stojkovic BP, Wolynes P (2000) The middle way. *Proc Natl Acad Sci USA* 97(1):32–37.
9. Schatz GC (2007) Using theory and computation to model nanoscale properties. *Proc Natl Acad Sci USA* 104(17):6885–6892.
10. Hu X, Damjanović A, Ritz T, Schulten K (1998) Architecture and mechanism of the light-harvesting apparatus of purple bacteria. *Proc Natl Acad Sci USA* 95(11): 5935–5941.
11. de la Lande A, Babcock NS, Rezác J, Sanders BC, Salahub DR (2010) Surface residues dynamically organize water bridges to enhance electron transfer between proteins. *Proc Natl Acad Sci USA* 107(26):11799–11804.
12. Wöbkenberg PH, et al. (2008) High mobility n-channel organic field-effect transistors based on soluble C60 and C70 fullerene derivatives. *Synth Met* 158:468–472.
13. Liu J, Zhang R, Sauvé G, Kowalewski T, McCullough RD (2008) Highly disordered polymer field effect transistors: N-alkyl dithieno[3,2-b:2′,3′-d]pyrrole-based copolymers with surprisingly high charge carrier mobilities. *J Am Chem Soc* 130(39): 13167–13176.
14. Zhang M, et al. (2007) Field-effect transistors based on a benzothiadiazole-cyclopentadithiophene copolymer. *J Am Chem Soc* 129(12):3472–3473.
15. Allard S, Forster M, Souharce B, Thiem H, Scherf U (2008) Organic semiconductors for solution-processable field-effect transistors (OFETs). *Angew Chem Int Ed Engl* 47(22): 4070–4098.
16. Abecasis GR, Cherny SS, Cookson WO, Cardon LR (2002) Merlin—Rapid analysis of dense genetic maps using sparse gene flow trees. *Nat Genet* 30(1):97–101.
17. Buldyrev SV, Parshani R, Paul G, Stanley HE, Havlin S (2010) Catastrophic cascade of failures in interdependent networks. *Nature* 464(7291):1025–1028.
18. Sylvester J (1878) Chemistry and algebra. *Nature* 17:284.
19. García-Domenech R, Gálvez J, de Julian-Ortiz JV, Pogliani L (2008) Some new trends in chemical graph theory. *Chem Rev* 108(3):1127–1169.
20. Holmes-Cerfon M, Gortler SJ, Brenner MP (2013) A geometrical approach to computing free-energy landscapes from short-ranged potentials. *Proc Natl Acad Sci USA* 110(1):E5–E14.
21. Beratan DN, et al. (2009) Steering electrons on moving pathways. *Acc Chem Res* 42(10):1669–1678.
22. Kekulé A (1865) Sur la constitution des substances aromatiques. *Bulletin de la Societe Chimique de Paris* 3(2):98–110.
23. Pauling L (1960) *The Nature of the Chemical Bond* (Cornell University Press, Ithaca, NY), 3rd Ed.
24. Clar E (1972) *The Aromatic Sextet* (J. Wiley & Sons, London).
25. Heilbronner E (1964) Huckel molecular orbitals of Mobius-type configurations. *Tetrahedron Lett* 5(29):923–1928.
26. Randić M (2003) Aromaticity of polycyclic conjugated hydrocarbons. *Chem Rev* 103(9): 3449–3605.
27. Estrada E, Hatano N (2007) Statistical-mechanical approach to subgraph centrality in complex networks. *Chem Physics Lett* 439(2007):247–251.
28. Burdett J, Lee S (1985) Moments and the energies of solids. *J Am Chem Soc* 107(11): 3050–3063.
29. Marcus RA (1993) Electron transfer reaction in chemistry. Theory and experiment. *Rev Mod Phys* 65(3):599–610.
30. Li G, Zhu R, Yang Y (2012) Polymer solar cells. *Nat Photonics* 6(3):153–161.
31. Lenes M, et al. (2008) Fullerene bisadducts for enhanced open-circuit voltages and efficiencies in polymer solar cells. *Adv Mater* 20:2116–2119.
32. Frost JM, Faist MA, Nelson J (2010) Energetic disorder in higher fullerene adducts: A quantum chemical and voltammetric study. *Adv Mater* 22(43):4881–4884.
33. Sharenko A, et al. (2013) A high-performing solution-processed small molecule:perylene diimide bulk heterojunction solar cell. *Adv Mater* 25(32):4403–4406.
34. Zhan X, et al. (2011) Rylene and related diimides for organic electronics. *Adv Mater* 23(2):268–284.
35. Savoie BM, et al. (2014) Unequal partnership: Asymmetric roles of polymeric donor and fullerene acceptor in generating free charge. *J Am Chem Soc* 136(7):2876–2884.
36. Klein D, Randić M (1993) Resistance distance. *J Math Chem* 12(1):81–95.
37. Lenes M, et al. (2009) Electron trapping in higher adduct fullerene-based solar cells. *Adv Funct Mater* 19:3002–3007.
38. Faist MA, et al. (2011) Effect of multiple adduct fullerenes on charge generation and transport in photovoltaic blends with poly(3-hexylthiophene-2,5-diyl). *J Polym Sci B Polym Phys* 49(1):45–51.
39. Rivnay J, et al. (2009) Large modulation of carrier transport by grain-boundary molecular packing and microstructure in organic thin films. *Nat Mater* 8(12):952–958.
40. Hansen MR, Graf R, Sekharan S, Sebastiani D (2009) Columnar packing motifs of functionalized perylene derivatives: Local molecular order despite long-range disorder. *J Am Chem Soc* 131(14):5251–5256.
41. Rajaram S, Shivanna R, Kandappa SK, Narayan KS (2012) Nonplanar perylene diimides as potential alternatives to fullerenes in organic solar cells. *J Phys Chem Lett* 3(17): 2405–2408.
42. Zhang X, et al. (2013) A potential perylene diimide dimer-based acceptor material for highly efficient solution-processed non-fullerene organic solar cells with 4.03% efficiency. *Adv Mater* 25(40):5791–5797.
43. Jiang W, et al. (2014) Bay-linked perylene bisimides as promising non-fullerene acceptors for organic solar cells. *Chem Commun (Camb)* 50(8):1024–1026.
44. Olds DP, Duxbury PM, Kiel JW, Mackay ME (2012) Percolating bulk heterostructures from neutron reflectometry and small-angle scattering data. *Phys Rev E Stat Nonlin Soft Matter Phys* 86(6 Pt 1):061803.
45. Li J, Ray B, Alam MA, Östling M (2012) Threshold of hierarchical percolating systems. *Phys Rev E Stat Nonlin Soft Matter Phys* 85(2 Pt 1):021109.
46. Groves C (2013) Developing understanding of organic photovoltaic devices: Kinetic Monte Carlo models of geminate and non-geminate recombination, charge transport and charge extraction. *Energy Environ Sci* 6:3202–3217.
47. Kwiatkowski JJ, Frost JM, Nelson J (2009) The effect of morphology on electron field-effect mobility in disordered c60 thin films. *Nano Lett* 9(3):1085–1090.
48. Rühle V, et al. (2011) Microscopic simulations of charge transport in disordered organic semiconductors. *J Chem Theory Comput* 7(10):3335–3345.
49. Baumeier B, Stenzel O, Poelking C, Andrienko D, Schmidt V (2012) Stochastic modeling of molecular charge transport networks. *Phys Rev B* 86:184202.